THE JOURNAL OF BIOLOGICAL CHEMISTRY VOL. 291, NO. 50, pp. 26138–26150, December 9, 2016

A Novel Role for Pyruvate Kinase M2 as a Corepressor for P53 during the DNA Damage Response in Human Tumor Cells*[S]

Received for publication, May 7, 2016, and in revised form, October 17, 2016 Published, JBC Papers in Press, November 3, 2016, DOI 10.1074/jbc.M116.737056

Li Xia[‡1], **Xin-Ran Wang**[‡1], **Xiao-Ling Wang**[‡], **Su-Hui Liu**[‡], **Xiao-Wei Ding**[‡], **Guo-Qiang Chen**[‡§2], **and Ying Lu**[‡3]

From the [‡]*Department of Pathophysiology, Key Laboratory of Cell Differentiation and Apoptosis of Ministry of Education, Shanghai Jiao Tong University School of Medicine (SJTU-SM), Shanghai 200025, China and the* [§]*Institute of Health Sciences, Shanghai Institutes for Biological Sciences of Chinese Academy of Sciences and SJTU-SM, Shanghai 200025, China*

Edited by Patrick Sung

The pyruvate kinase (PK) is a rate-limiting glycolytic enzyme catalyzing the dephosphorylation of phosphoenolpyruvate to pyruvate, yielding one molecule of ATP. The M2 isoform of PK (PKM2) is predominantly expressed in normal proliferating cells and tumors, and both metabolic and non-metabolic activities for the enzyme in promoting tumor cell proliferation have been identified. However, the exact roles of PKM2 in tumor initiation, growth and maintenance are not yet fully understood. Using immunoprecipitation-coupled LC-MS/MS in MCF7 cells exposed to DNA-damaging agent, we report that the nuclear PKM2 interacts directly with P53 protein, a critical safeguard for genome stability. Specifically, PKM2 inhibits P53-dependent transactivation of the *P21* gene by preventing P53 binding to the *P21* promoter, leading to a nonstop G_1 phase. As a result, PKM2 expression provides a growth advantage for tumor cells in the presence of a DNA damage stimulus. In addition, PKM2 interferes with phosphorylation of P53 at serine 15, known to stimulate P53 activity by the ATM serine/threonine kinase. These findings reveal a new role for PKM2 in modulating the DNA damage response and illustrate a novel mechanism of PKM2 participating in tumorigenesis.

Pyruvate kinase (PK),[4] a rate-limiting enzyme of glycolysis, catalyzes the transfer of phosphate from phosphoenolpyruvate (PEP) to ADP, yielding one molecule of ATP and pyruvate. The PK consists of four isoforms, the *PKLR* gene-encoded PKL and PKR isoforms and the *PKM* gene-encoded M1 (PKM1) and M2 (PKM2) isoforms, which express in different types of mammalian cells and tissues. PKM1 constitutively forms stable tetramers (the active form of PK) and is expressed in normal adult tissues that require high levels of energy, such as the heart, brain, and skeletal muscle. In contrast, PKM2 exists in either tetramers or dimers with less activity and metabolic intermediate fructose-1,6-bisphosphate (FBP) can allosterically activate PKM2 by promoting the formation of tetramer from dimer (1, 2). PKM2 is selectively expressed in normal proliferating cells as well as tumor cells, indicating an indispensable role in cancer development.

There are two known mechanisms by which PKM2 favors tumor cell growth, one dependent on and one independent of glycolysis. As a glycolytic enzyme, PKM2 in tumor cells shifts glucose metabolism from oxidative phosphorylation to glycolysis under normoxic conditions, a phenomenon termed the Warburg effect or aerobic glycolysis (3). On the other hand, non-metabolic function of PKM2, which is mainly associated with the nuclear PKM2, has been identified as a major contributor during tumorigenesis. For example, nuclear PKM2 displays kinase activity in phosphorylating a number of protein substrates, including histone H3 (4, 5), signal transducer and activator of transcription 3 (stat3) (6, 7), Bub3 (8), and myosin light chain 2 (MLC2) (9), for which PKM2 uses the high-energy phosphate from PEP but not ATP as a phosphate donor. The PKM2-induced phosphorylations of stat3 at tyrosine 705 and histone H3 at threonine 11 respectively activate the transcriptions of *MEK5* and endothelial growth factor (EGF)-stimulated *cyclin D1*, leading to increased tumor cell proliferation. Intriguingly, the dimeric form of PKM2 which predominantly exists in cancer cells is also be reported to bias the protein kinase function toward stat3 (6). Moreover, recent studies showed that PKM2 can function as a coactivator of hypoxia-inducible factor-1α (HIF-1α) and β-catenin under hypoxia or EGF treatment (10, 11). These data indicate that PKM2 plays an important role in promoting tumor development through regulating gene transcriptions. However, there were also some controversies regarding the function of PKM2 in tumor growth, which have complicated the mechanism of PKM2-related tumorigenesis (12–16). For example, *in vivo* growth of established xenograft tumors with HCT116 or RKO colon carcinoma cells is unaffected by PKM2 knockdown (12). Also, PKM2 deletion was shown to accelerate tumor formation in a spontaneous breast cancer model (13). Therefore, the exact roles of PKM2 in tumor growth and maintenance are not yet fully understood.

* This work was supported by National Key Research Program of China (NO2015CB910403), National Natural Science Foundation (81370652, 81230048, 81430061, 31570824), Foundation for the author of National Excellent Doctoral Dissertation of China (201074), Grants from Science and Technology Committee of Shanghai (13431900501) and Talent Development Project of Shanghai Human Resource and Social Security Bureau. The authors declare that they have no conflicts of interest with the contents of this article.

[S] This article contains supplemental Tables S1–S3.

[1] Both authors contributed equally to this work.

[2] To whom correspondence may be addressed: No. 280, Chong-Qing South Rd., Shanghai, 200025, China. Tel./Fax: +86-21-64154900; E-mail: chengq@shsmu.edu.cn.

[3] To whom correspondence may be addressed: No. 280, Chong-Qing South Rd., Shanghai, 200025, China. Tel./Fax: +86-21-64154900; E-mail: stove@shsmu.edu.cn.

[4] The abbreviations used are: PK, pyruvate kinase; PEP, phosphoenolpyruvate; GO, gene ontology; ATM, ataxia telangiectasia mutated; NC, negative control; HIF, hypoxia-inducible factor; RE, responsive element.

P53 tumor suppressor is a critical guardian of genome stability. It responds to various DNA damage stimuli and maintains at low levels in unstressed mammalian cells because of MDM2-mediated ubiquitylation and degradation (17, 18). Upon the stress, P53 is modified by multiple post-transcriptional mechanisms, such as phosphorylation at serine(Ser) 15 by the serine threonine kinase ataxia-telangiectasia mutated (ATM), which leads to its dissociation from its negative regulator MDM2, followed by the accumulation and activation of P53 (19). The activated P53 upon DNA damage plays a central role in the decision of a cell to undergo cell cycle arrest or apoptosis by activating downstream target genes. Dysfunction of P53 contributes to and occurs during the development of most tumor types (20). Herein, we identified PKM2 functions as a corepressor for P53 during DNA damage response (DDR), leading to decreased expression of P21 together with continued growth of tumor cells.

Results

Identification of Nuclear PKM2-interacting Proteins in DNA-damaged or Undamaged Cancer Cells—We first detected the expression and distribution of PKM2 in MCF7 breast cancer cells with or without the treatment of etoposide (VP16), a DNA-damaging agent. As consistent with the previous reports (10, 11), most of PKM2 were localized in the cytoplasm with a small fraction in the nuclei, and etoposide treatment did not change PKM2 protein level and its cytoplasmic/nuclear distribution in MCF7 cells (Fig. 1*A*). To explore the potential functions of nuclear PKM2 in response to etoposide treatment, we fractionated the nuclear extracts of etoposide-treated and untreated MCF7 cells by size-exclusion chromatography, followed by detection of PKM2 protein. The results demonstrated that, consistent with previous findings in most cancer cells (3, 21–23), nuclear PKM2 predominantly existed in low-molecular-weight fractions (fractions 41–45) corresponding to PKM2 dimer. Unexpectedly, an aliquot part of nuclear PKM2 also existed in a high-molecular-weight (>669 kDa) fractions (fractions 24–28) (*upper panel*, Fig. 1*B*), suggesting that nuclear PKM2 can form large complexes with other proteins. More intriguingly, etoposide treatment made the high-molecular-weight fractions shift to fractions 26–31 (*bottom panel*, Fig. 1*B*), although it did not change the formation of PKM2 dimer (fractions 41–45). Hence, we extrapolated formation of different nuclear PKM2 complexes in response to DNA damage. To confirm this, we used anti-PKM2 antibody with the non-related IgG as a control to precipitate nuclear fractions 22–26 and 27–31, respectively, and their precipitates were analyzed by liquid chromatography-mass spectrometry/mass spectrometry (LC-MS/MS) (Fig. 1*C*). We recognized a unique peptide (aa401–422), which belongs to PKM2 but not PKM1, and histone H3, a previously reported PKM2-interacting protein (4) (Fig. 1*D*), supporting the specificity and effectiveness of the co-immunoprecipitation (co-IP) assay. Totally, anti-PKM2 but not IgG pulled down 133 and 91 non-redundant proteins respectively in etoposide-untreated and treated MCF7 cells (Fig. 1*E* and supplemental Tables S1 and S2). Among these anti-PKM2 pulled down proteins, 90 and 48 proteins exclusively appeared, respectively, in etoposide-untreated and treated nuclear extracts. In particular, there were 43 proteins presented in both extracts, in which 13 proteins shifted between fractions 22–26 and 27–31 upon etoposide treatment (Fig. 1*F* and supplemental Table S2). Gene Ontology analysis showed that these PKM2-interacting proteins are involved in various nuclear events including DDR (supplemental Table S3). P53, the key effector in DNA damage signaling (24), was also identified in nuclear PKM2 complexes in etoposide-treated fraction (Fig. 1*D*). Furthermore, protein-protein interaction network based upon the identified nuclear PKM2-interacting DDR-related proteins constructed by String database showed that PKM2-interacting proteins from etoposide-treated MCF7 cells created a more complicated network compared with untreated ones (Fig. 1*G*), in which P53 had more than 3 edges, suggesting that P53 is one of the key proteins contributing to PKM2-related DDR.

PKM2 Interacts with P53—MCF7 expressed wild type *P53* (P53-WT) gene (25, 26), as confirmed by sequencing in the present study (data not shown). As described in the previous reports (17, 18), P53 protein was expressed at low level and could be accumulated by etoposide treatment in MCF7 cells (Fig. 2*A*), which could be seen in immunofluorescent assay (Fig. 2*B*). To confirm the interaction between PKM2 and P53, we showed that the P53 protein could be precipitated by anti-PKM2 antibody in etoposide-treated MCF7 cells (*top*, Fig. 2*A*). Reciprocally, anti-P53 antibody could precipitate PKM2 protein (*bottom*, Fig. 2*A*). The PKM2-P53 interaction was also found by co-IP in human colon cancer HCT116 cells and osteosarcoma U2OS cells (Fig. 2*C*). Next, size-exclusion chromatography assay showed that purified P53 could co-elute with recombinant PKM2 mainly at fractions 36~38 corresponding to 200–300 kDa, demonstrating their direct interaction (Fig. 2*D*).

To define the binding domains of PKM2 and P53 for their interaction, bacterially expressed GST-tagged P53 and/or His-tagged PKM2 and their fragments were applied for *in vitro* pull-down assays (27). As depicted in Fig. 2*E*, full-length P53 and its DNA binding domain (DBD, aa102–300) pulled down PKM2 to the similar efficacy. Further, the fragment 201–393 but not fragments 1–43 and 1–200 as well as 300–393 of P53 still pulled PKM2 down. Therefore, we concluded that C-terminal moiety (aa201–300) of DBD of P53 was essential for its interaction with PKM2. On the other direction, the domains C (aa390–531), A1 (aa45–116), and A2 (aa219–389) of PKM2 appeared to be able to interact with P53 (Fig. 2*F*). Competition binding analysis demonstrated that the PEP significantly inhibited PKM2 binding to P53, suggesting the competition of PEP with P53 in binding PKM2 (Fig. 2*G*). Moreover, tetrameric PKM2 displayed a higher binding affinity to P53 than its dimeric form (Fig. 2*H*), which could be further supported by GST-pull down assay with dimer-forming PKM2-R399E mutant (Fig. 2*I*) (6).

PKM2 Inhibits Transcriptional Activity of P53—As well documented (17, 18, 28), P53 is stabilized and transcriptionally activated through multiple post-translational modifications including phosphorylation upon DNA damage. For example, ATM or ataxia telangiectasia mutated and Rad3-related (ATR)-induced phosphorylation at Ser-15 and Ser-20 is one of the important mechanisms responsible for DNA damage-accumulated P53 protein (19, 30–31). We continue to address

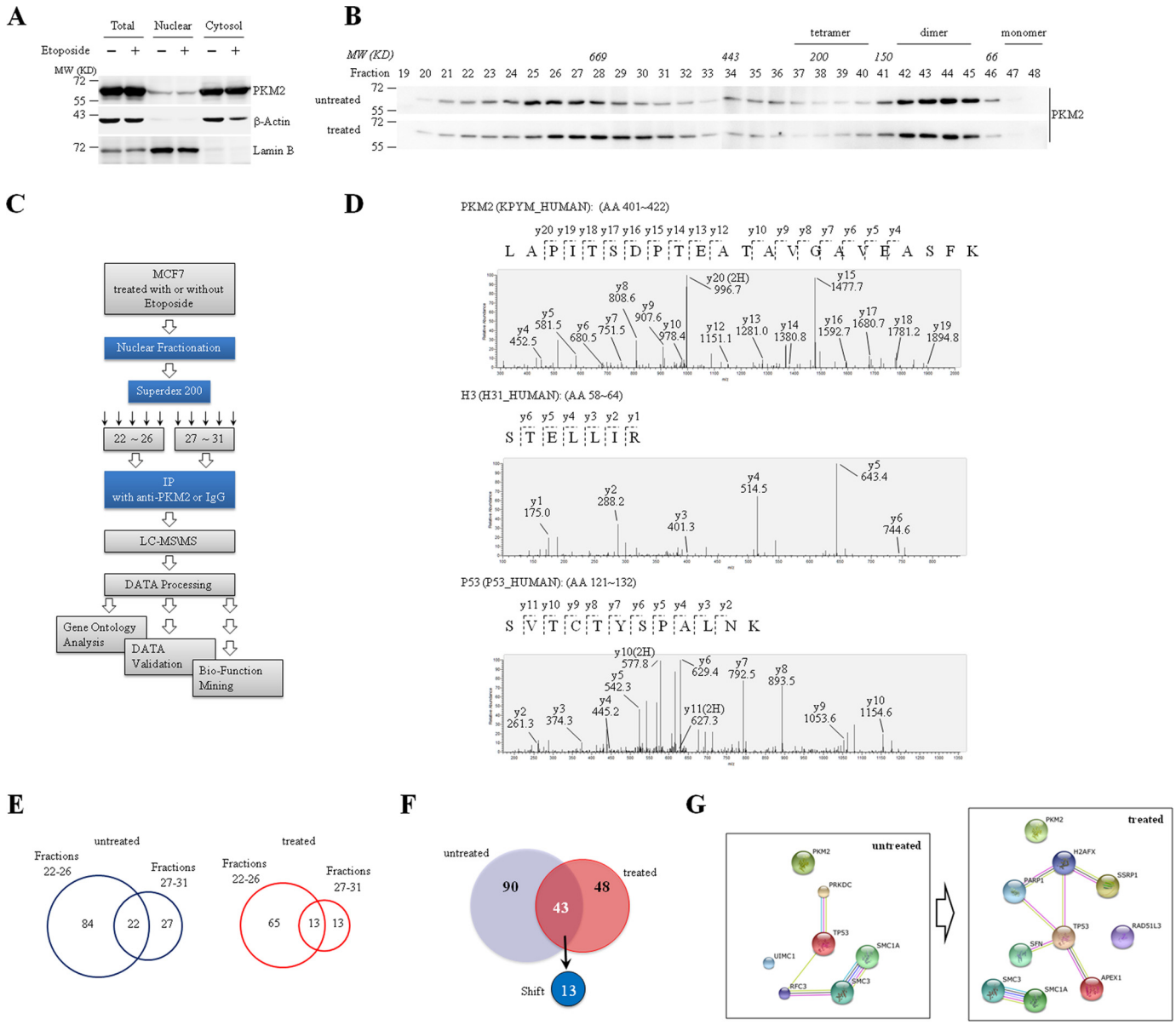

FIGURE 1. **Identification of nuclear PKM2-interacting proteins in DDR.** *A*, cytosolic and nuclear extracts were prepared from MCF7 cells treated with or without etoposide, followed by Western blot analysis for the indicated proteins. LaminB was a nuclear marker, and *β*-actin acted as a cytosol marker. *B*, size-exclusion chromatography analysis of nuclear extracts from MCF7 cells with or without treatment of etoposide for 8 h, followed by immunoblotting with anti-PKM2 antibody. *C*, experimental strategy and workflow for identification of PKM2-interacting proteins in response to DNA damage. *D*, MS-MS spectra of representative peptides, including PKM2 (an exclusive peptide within the exon 10 of PKM2), Histone H3, and P53. *E*, the Venn diagram of nuclear PKM2-interacting proteins separated by superdex 200 in fractions 22–26 or 27–31 identified in MCF7 cells with and without treatment of etoposide. *F*, the Venn diagram displaying the numbers of identified PKM2-interacting proteins in MCF7 cells treated or untreated with etoposide for 8 h. Out of the 43 proteins identified in both groups, 13 proteins shift between fractions 22–26 and 27–31 in response to etoposide treatment. *G*, analysis of the PKM2-interacting DNA damage-related proteins in MCF7 cells treated or untreated with etoposide for 8 h by String database. All the proteins shown are not yet reported DDR-related PKM2-interacting proteins indentified by LC-MS/MS. The edge indicates known interaction between two proteins.

whether PKM2 regulates P53 activity. To this end, a pair of small hairpin RNAs (shRNAs) specifically against PKM2 (shPKM2#1) was transfected into MCF7 cells, together with a nonspecific shRNA as a negative control (NC). While etoposide accumulated equivalent P53 protein in both NC and shPKM2#1-infected MCF7 cells (Fig. 3*A*), PKM2 silencing significantly elevated Ser 15 phosphorylation of P53 upon etoposide treatment (Fig. 3*A*), which has been documented as a transcriptional active form of P53 (19, 30). Similar phenomena could also be seen in HCT116 and U2OS cells (Fig. 3, *B* and *C*). To further consolidate the specific effect of PKM2 on Ser-15 phosphorylation of P53, we re-expressed PKM2-WT as well as its R399E mutant in MCF7 cells, and found that restored PKM2-WT inhibited Ser-15 phosphorylation of P53 after etoposide treatment (Fig. 3*D*). Introduction of the dimer-forming PKM2-R399E mutant, however, induced a comparable level of Ser-15 phosphorylation of P53 with that of PKM2-depleted EV group after etoposide treatment (Fig. 3*D*), indicating that PKM2-R399E mutant lacks impacts on P53 due to weak binding capacity to P53 in cells. Of note, Ser-20 phosphorylation of P53 was not detectable in MCF7 cells (Fig. 3*A*).

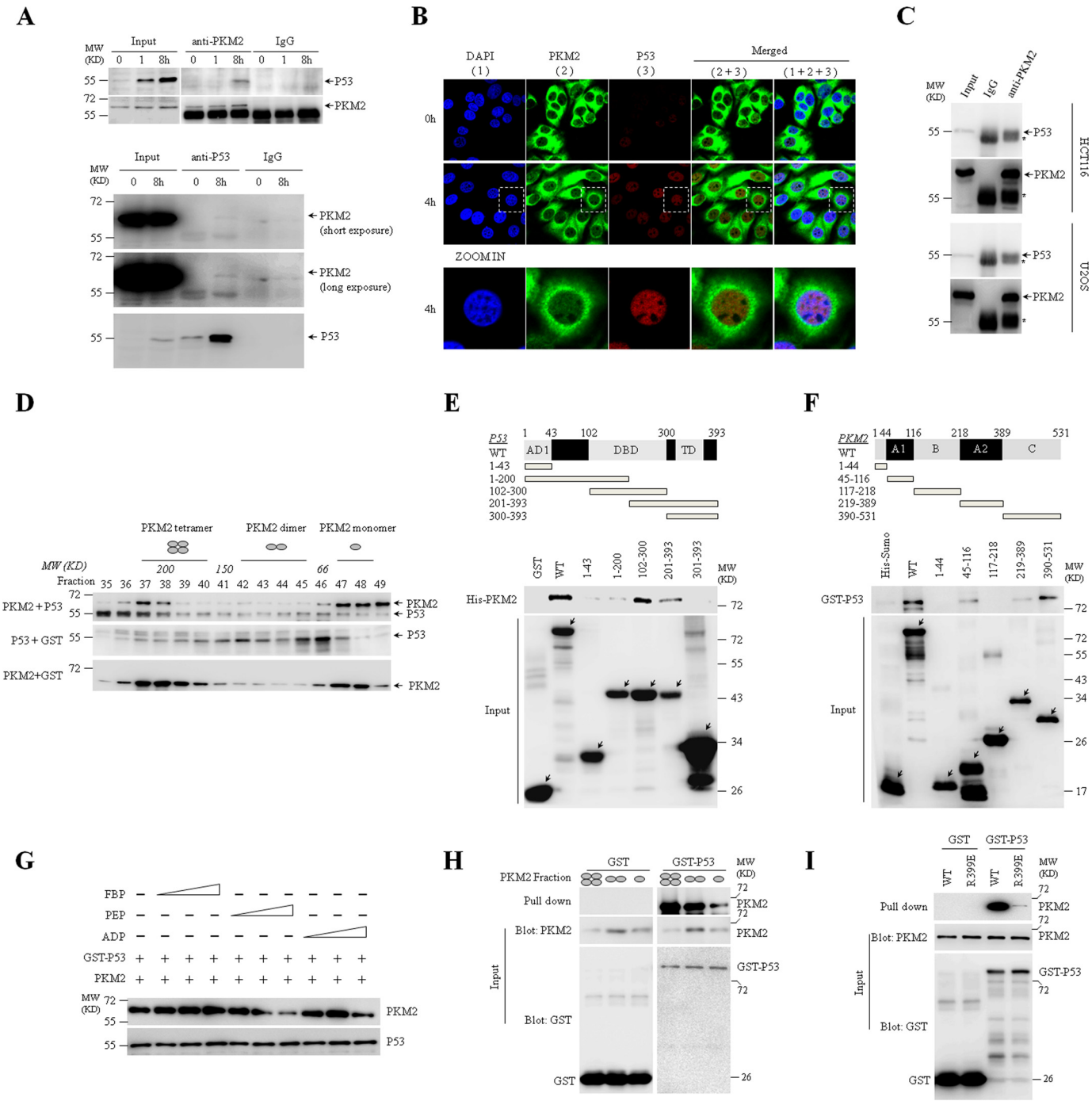

FIGURE 2. **PKM2 directly interacts with P53.** *A*, co-IP analysis of the interaction between endogenous P53 and PKM2 using anti-PKM2 or anti-P53 antibody in MCF7 cells treated with or without etoposide for the indicated hours. IgG was a negative control. Input, 10% the whole cell lysate. *B*, immunofluorescent staining of endogenous PKM2 and P53 in MCF7 cells treated with or without etoposide for 4 h. Antibodies against total PKM2 or P53 were used. The *bottom panel* showed the amplified images for cells lined with white lines. *C*, co-IP analysis of the interaction between endogenous P53 and PKM2 using anti-PKM2 antibody in HCT116 and U2OS cells treated with etoposide for 8 h. IgG was a negative control. Input, 10% the whole cell lysate. * represents the heavy chain of antibody. *D*, size-exclusion chromatography analysis of interaction between recombinant PKM2 and P53. According to the molecular weight, the four, two, or one ellipse represents tetramer, dimer, or monomer of PKM2, respectively. *E* and *F*, GST pull-down analysis of interaction between PKM2 and P53 subunits containing the indicated amino acid residues using purified His-tagged PKM2 and GST-tagged P53 fusion proteins. Full-length (WT) or the truncated segments were illustrated by structure schematic diagram. *AD1*, activation domain 1; *DBD*, DNA binding domain; *TD*, transcriptional domain. *G*, GST pull-down analysis of GST-P53 with PKM2 in the presence of the escalating concentrations (10/100/1,000 μM) of FBP, PEP or ADP. *H*, GST pull-down analysis of GST or GST-P53 with PKM2 tetramer (fraction 38), dimer (43), and monomer (47) isolated by size exclusion chromatography. *I*, GST pull-down analysis of interaction between P53 and PKM2-WT or PKM2-R399E mutant, followed by immunoblotting with indicated antibodies. All these experiments were repeated at least for three times with the same results.

In line with the increased Ser-15 phosphorylation, the specific P53 responsive element (RE)-driven luciferase assay showed that knockdown of PKM2 significantly increased transcriptional activity of P53 in MCF7 cells under 4-h treatment of etoposide (Fig. 3*E*). To elucidate the mechanism underlying the inhibitory effect of PKM2 on P53 transcription, we conducted

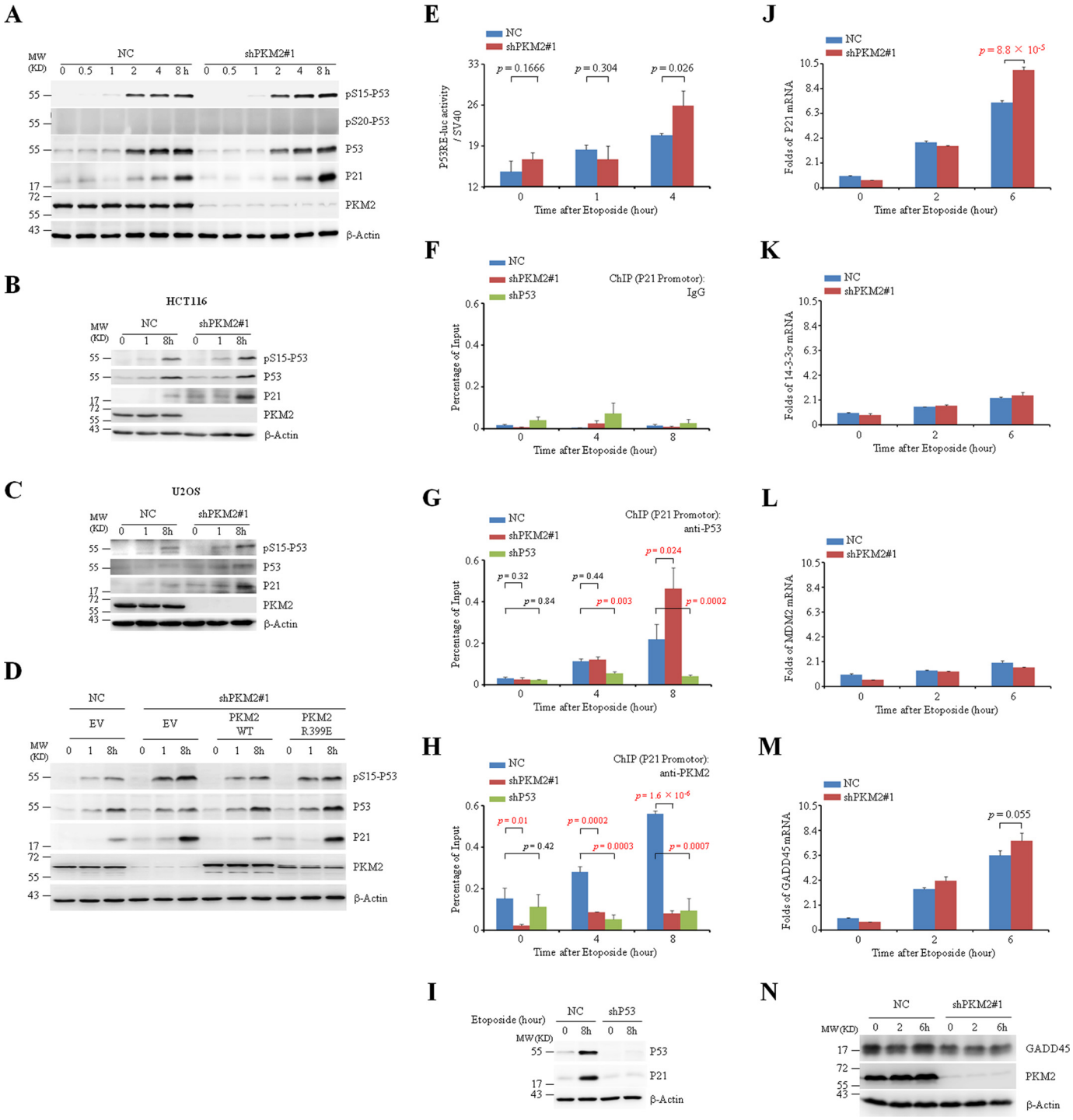

FIGURE 3. **PKM2 inhibits transcriptional activity of P53.** *A*, negative control (*NC*) or shPKM2#1-infected MCF7 cells were treated with etoposide for the indicated hours, followed by immunoblotting. The pS15 or pS20-P53 indicates P53 protein phosphorylated at serine 15 or 20. *B* and *C*, NC or shPKM2#1-infected HCT116 (*B*) and U2OS (*C*) cells were treated with etoposide for the indicated hours followed by immunoblots for the indicated proteins. *D*, MCF7 cells reconstitutively expressing empty vector (EV), PKM2-WT, or PKM2-R399E mutant were treated with etoposide for the indicated hours. Immunoblotting was detected for the indicated proteins. *E*, NC or shPKM2#1-infected MCF7 were transfected with plasmids p53-TA-firefly-luc reporter and control reporter pSV40-Renilla, followed by treatment with etoposide for 0, 1, or 4 h, and the relative luciferase activity were determined. *F–H*, NC, shP53 or shPKM2#1-infected MCF7 cells were exposed to etoposide for the indicated hours. ChIP assays were performed with IgG (*F*), anti-P53 (*G*), and anti-PKM2 antibody (*H*). *I*, MCF7 cells infected with NC or shP53 were exposed to etoposide for the indicated hours. Immunoblotting was detected for the indicated proteins. *J–M*, real-time quantitative PCR analysis of mRNAs of P21 (*J*), 14-3-3σ (*K*), MDM2 (*L*), and GADD45 (*M*) in the NC or shPKM2#1-infected MCF7 cells treated with etoposide for the indicated hours. Relative folds of mRNA were normalized to the value in untreated NC-infected cells. *N*, Western blot analysis of GADD45 in the NC or shPKM2#1-infected MCF7 cells treated with etoposide for the indicated hours.

chromatin immunoprecipitation (ChIP) assays. The results revealed that anti-P53 rather than non-related IgG could pull down P53RE of the promoter of *P21* gene, which was disappeared in P53 silencing cells (Fig. 3, *F*, *G*, and *I*), indicating the effectiveness and specificity of our ChIP assay. Of more significance, anti-PKM2 antibody could precipitate the P53RE of the

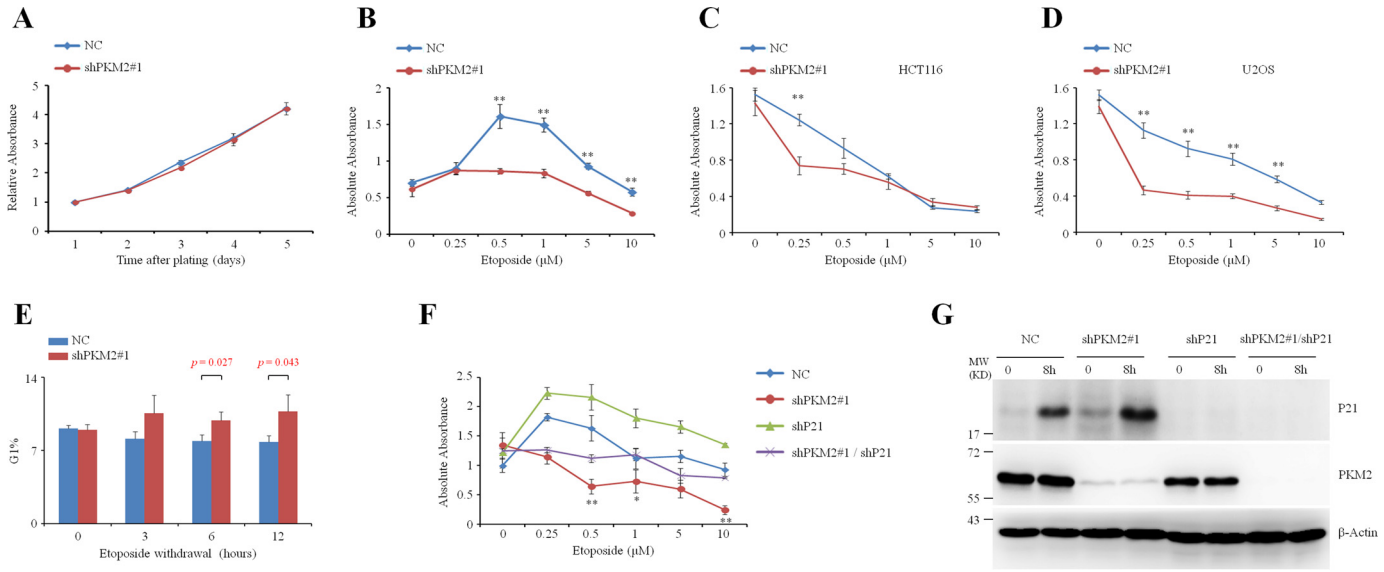

FIGURE 4. **Knockdown of PKM2 enhanced cell cycle arrest in response to DNA damage.** *A*, CCK-8 assay of cell proliferation in the NC or shPKM2#1-infected MCF7 cells for 5 days. Data are presented as means ± S.D. *B–D*, MCF7 (*B*), HCT116 (*C*), and U2OS (*D*) cells infected with NC or shPKM2#1 were exposed to a spectrum of etoposide for 3 days and were subjected to CCK-8 assay. **, $p < 0.01$ *versus* shPKM2#1. Data are presented as means ± S.D. *E*, MCF7 cells infected with NC or shPKM2#1 were treated with low dose (5 μM) of etoposide for 3 days before etoposide withdrawal. The cells were subjected to flow cytometry analysis at 0, 3, 6, 12 h after etoposide withdrawal. The quantification of G1 phase was shown. Data are presented as means ± S.D. *F*, MCF7 cells infected with NC, shPKM2#1 or/and shP21 were exposed to a spectrum of etoposide for 3 days and were subjected to CCK-8 assay. **, $p < 0.01$; *, $p < 0.05$ *versus* shPKM2#1/shP21. *G*, MCF7 cells infected with NC, shPKM2#1 or/and shP21 were treated with etoposide and subjected to Western blot analysis.

promoter of *P21* gene under etoposide treatment, which could not be seen in PKM2-silencing cells (Fig. 3*H*). Furthermore, PKM2 occupancy at the P53RE was blocked by P53 silencing, suggesting that PKM2 was recruited to P53RE through P53 (Fig. 3*H*). More importantly, PKM2 knockdown significantly increased binding of P53 to P53RE within the *P21* promoter after etoposide treatment for 8 h (Fig. 3*G*). In line with this, PKM2 knockdown increased mRNA and protein expressions of P21, a P53-targeted gene and cyclin-dependent kinase inhibitor, upon etoposide exposure, although such induction could not be seen for several other P53-targeted genes including *14–3-3σ*, *MDM2* and *GADD45* (Fig. 3, *A* and *J–N*). Taken together, these data suggest that PKM2 inhibits the transcriptional activity of P53.

PKM2 Promotes Tumor Growth under DNA Damage—The increased P21 expression in the PKM2 depletion prompted us to detect the possible effects of PKM2 in cell proliferation under DNA damage stimulus. Our results showed that knockdown of PKM2 *per se* did not cause apparent change in either cell cycle (data not shown) or proliferation without etoposide treatment (Fig. 4*A*). However, PKM2-depleted MCF7 (Fig. 4*B*), HCT116 (Fig. 4*C*), and U2OS (Fig. 4*D*) cells showed a decreased proliferation under the treatment of etoposide at different concentrations, as evaluated by cell counting kit-8 (CCK-8) assay. Additionally, cell cycle was arrested at G_1 phase in PKM2-depleted MCF7 cells after the withdrawal of etoposide exposure for 3 days (Fig. 4*E*). These data suggested that PKM2 endows cancer cells with the capability to continue to grow in the presence of DNA damage. To evaluate whether P21 is required for the effect of PKM2 on cell proliferation, we knocked P21 down in PKM2-depleted cells, and the results showed that knockdown of P21 partially restored the proliferation of PKM2-depleted MCF-7 cells (Fig. 4, *F* and *G*), indicating that P21 participates in the function of PKM2 on cell proliferation.

To investigate the effect of PKM2 on tumor growth *in vivo*, luciferase-labeled MCF7 cells infected with NC or shPKM2#1 were injected into the mammary fat pad of the nude mice and luciferase photon fluxes were monitored before and after injection of etoposide or DMSO. The representative noninvasive bioluminescent images (BLI) from 5 mice are shown (Fig. 5, *A–D*). Consistent with the *in vitro* findings, xenograft experiments showed no significant difference between tumors generated from the NC and shPKM2-infected MCF7 cells without etoposide treatment (Fig. 5, *A* and *C*). When the mice experienced a period of chemotherapy with etoposide, the average volumes of tumors generated from NC-infected MCF7 cells were much bigger than that of shPKM2-infected ones (Fig. 5, *B* and *D*). Western blots showed that compare with NC tumors, administration of etoposide led to increased Ser-15 phosphorylation of P53 in shPKM2 tumors (Fig. 5*E*), suggesting that PKM2 modulates Ser-15 phosphorylation of P53 *in vivo*.

Since PKM2 catalyzes the final step in glycolysis, we measured the level of PEP, pyruvate, lactate as well as glucose uptake using fluorescent (green) glucose analog 2-[*N*-(7-nitrobenz-2-oxa-1,3-diazol-4-yl) amino]-2-deoxy-D-glucose (2-NBDG). As shown in Fig. 6*A*, knockdown of PKM2 in MCF-7 cells led to a decrease of glucose uptake. Cellular PEP increased vaguely in accompany with decreased level of lactate and pyruvate, indicating a slight decrease of glycolytic pyruvate kinase activity in PKM2-depleted cells, which might be due to the enzyme activity of PKM2 (Fig. 6, *B–D*). Compared with the drastic reduction of PKM2 protein (Fig. 3*A*), however, the changes in metabolism are imperceptible. Moreover, no obvious change in glucose uptake was observed upon etoposide treatment (Fig. 6*E*), suggesting that the differences in cell growth induced by PKM2 depletion were not attributable to the alteration in glucose metabolism. In addition, considering the interaction between P53 and PKM2, we measured PKM2 activity in MCF7 cells with

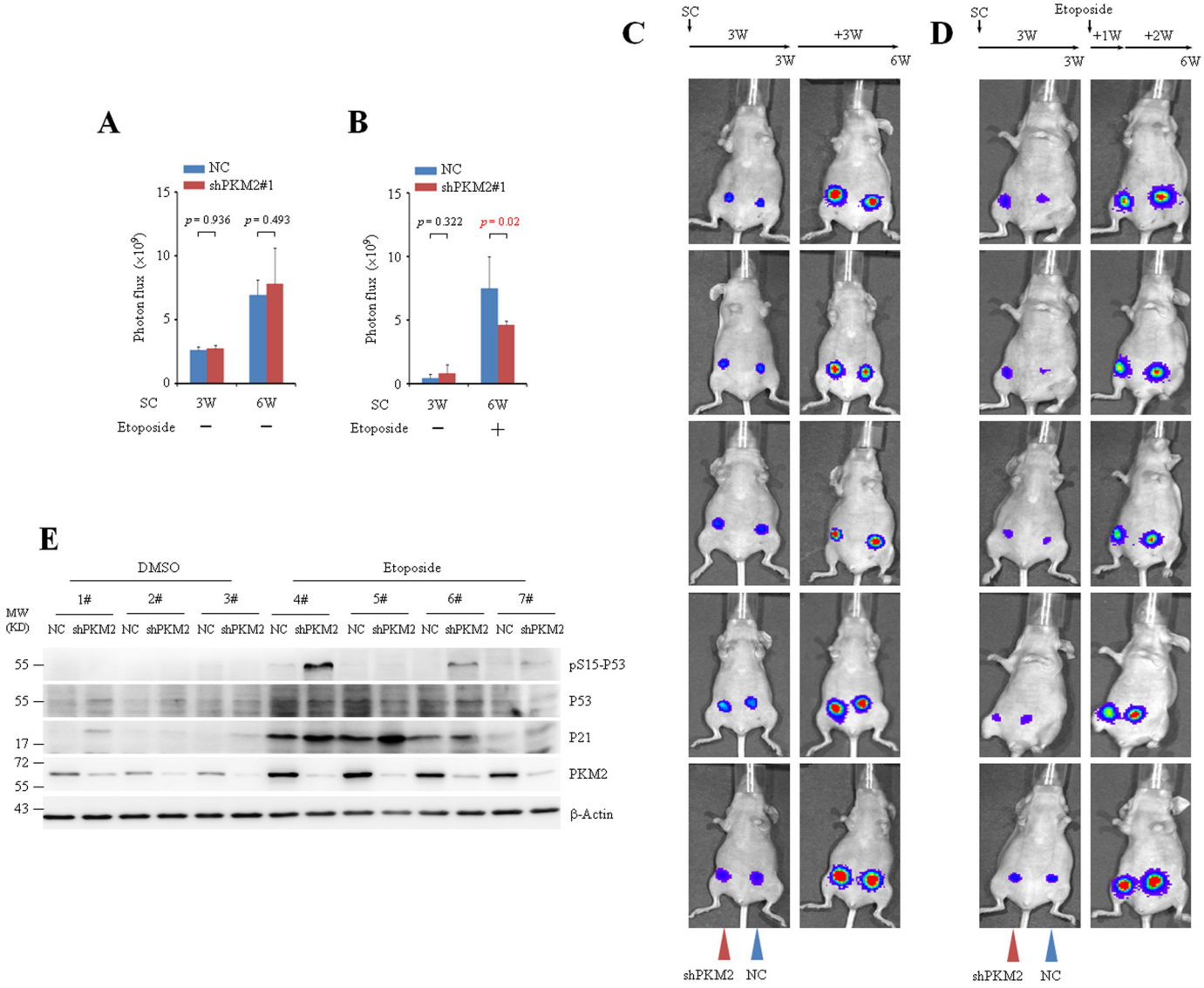

FIGURE 5. **PKM2 promotes tumor growth under DNA damage stimulus.** *A–D*, MCF7 cells infected with NC or shPKM2#1 were injected subcutaneously (*SC*) into the left (*NC*) or right (*shPKM2*) side of the mammary fat pad of the nude mice. Three weeks postinjection, imaging was performed using the Xenogen IVIS Imaging System. Afterward, a dose of 0.1 mg/kg of etoposide was administrated intraperitoneally for 7 consecutive days. Two weeks later, bioluminescent imaging was performed (*D*). The control mice were administrated with DMSO in parallel (*C*). The representative noninvasive bioluminescent images from 5 mice are shown. *A* and *B*, quantification of tumor burdens identified by bioluminescence imaging. Data are presented as means ± S.D. All these experiments were repeated at least for three times with the same results. *E*, MCF7 cells infected with NC or shPKM2#1 were injected into the left or right side of the mammary fat pad of nude mice and grown for 3 weeks. Afterward, a dose of 0.1 mg/kg of etoposide was administrated intraperitoneally for 7 consecutive days. Two weeks later, the fresh tumors from the mice were collected, homogenated and subjected to Western analysis with the indicated antibodies.

or without P53. As shown in Fig. 6*F*, compared with NC cells, knockdown of P53 did not change the protein level of PKM2 (*right panel*) but increased the pyruvate kinase activity (*left panel*) of MCF7 cells, indicating that P53 may inhibit the pyruvate kinase activity of PKM2.

PKM2 Inhibits the Kinase Activity of ATM on P53—We next investigated how PKM2 influences the phosphorylation of P53 at Ser-15 in response to DNA damage. As described above, several effector kinases functioning in DDR such as ATM can phosphorylate P53 at Ser-15, which is a key step in transducing DNA damage signaling (19, 30, 32). Thus, we detected the potential association of PKM2 and ATM on P53 phosphorylation upon DNA damage. As shown in Fig. 7*A*, recombinant PKM2 dose-dependently inhibited ATM-induced Ser-15 phosphorylation of P53 in the presence of ATP. Furthermore, both PKM2 and ATM from MCF7 cell lysates could be pulled down by purified GST-P53 (Fig. 7*B*). His-tagged PKM2 also precipitated Ser 1981-phosphorylated ATM in the presence or absence of P53 (Fig. 7*C*), suggesting an interaction between PKM2 and ATM. Immunoprecipitation with anti-Ser-1981-phosphorylated ATM antibody further confirm the interaction between endogenous PKM2 and ATM (Fig. 7*D*). In addition, considering the protein kinase activity of PKM2 that has been reported in a number of recent studies (4–6, 33), we extrapolated that P53 might be directly phosphorylated by PKM2. *In vitro* kinase assay demonstrated that PKM2 failed to directly induce phosphorylation of P53 in the presence of PEP or ATP (Fig. 7*E*). Collectively, these data suggest that PKM2 interfered with the kinase activity of ATM toward P53 at Ser-15 through a potential direct interaction.

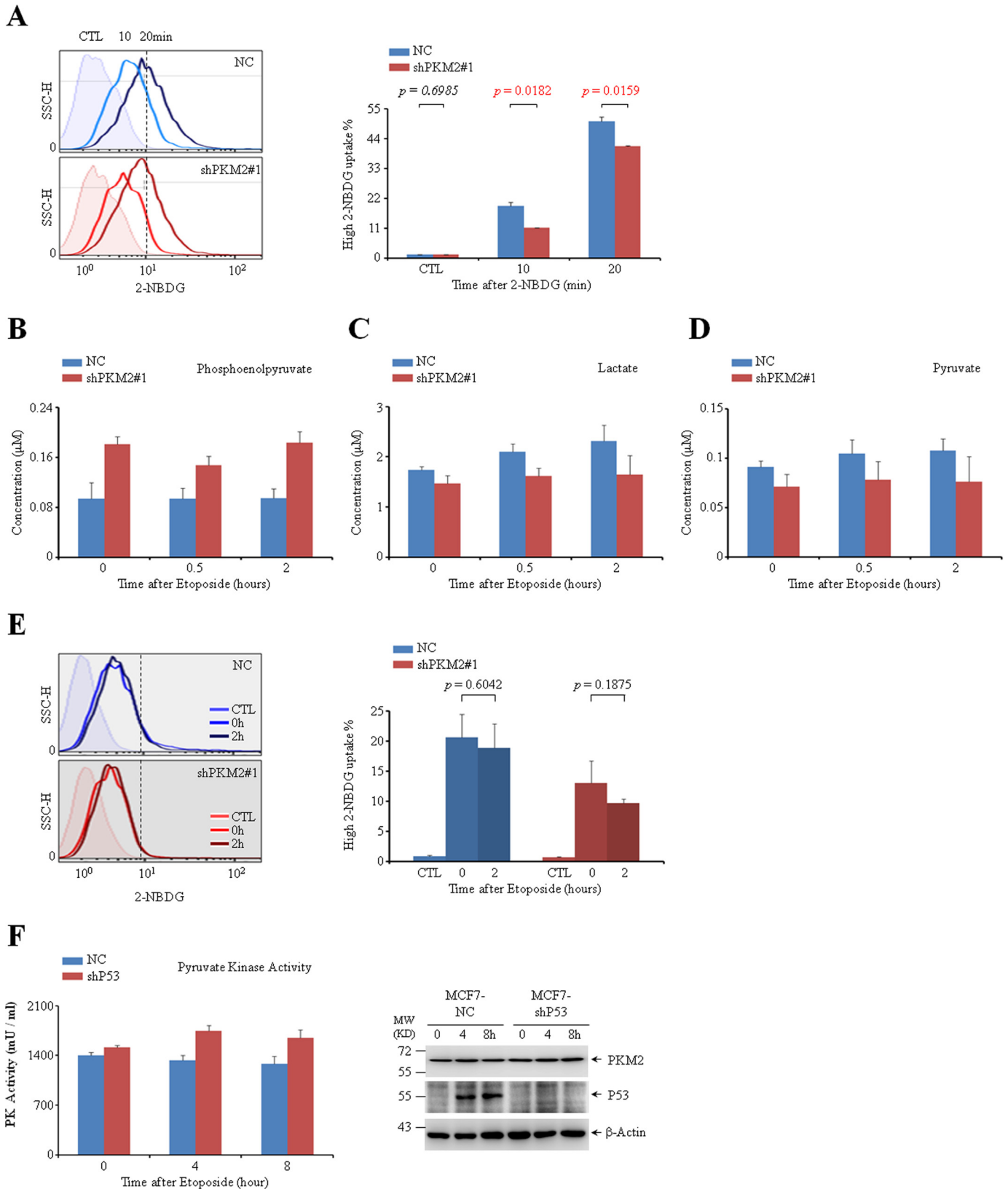

FIGURE 6. **The catalytic activity of PKM2 in response to DNA damage stimuli.** *A*, flow cytometric analysis of glucose uptake in MCF7 cells infected with NC or shPKM2#1 after the cells were incubated with 2-NBDG for 10 or 20 min. CTL (control) represents data of negative control collecting from cells without 2-NBDG incubation. The cells on the right of the *dotted lines* were defined as ones with the relative high 2-NBDG uptake, and their percentages were shown. *B–D*, fluorometric measurement of the relative concentration of PEP (*B*), lactate (*C*), and pyruvate (*D*) in MCF7 cells infected with NC or shPKM2#1 followed by treatment with etoposide for 0, 0.5, or 2 h. *E*, flow cytometric analysis of glucose uptake in MCF7 cells infected with NC or shPKM2#1 and treated with or without etoposide for 2 h. The percentages of cells with the relative high 2-NBDG uptake were quantified and shown on the *right*. *F*, fluorometric measurement of the pyruvate kinase activity (*left panel*) and Western blot analysis (*right panel*) of MCF7 cells infected with NC or sh53.

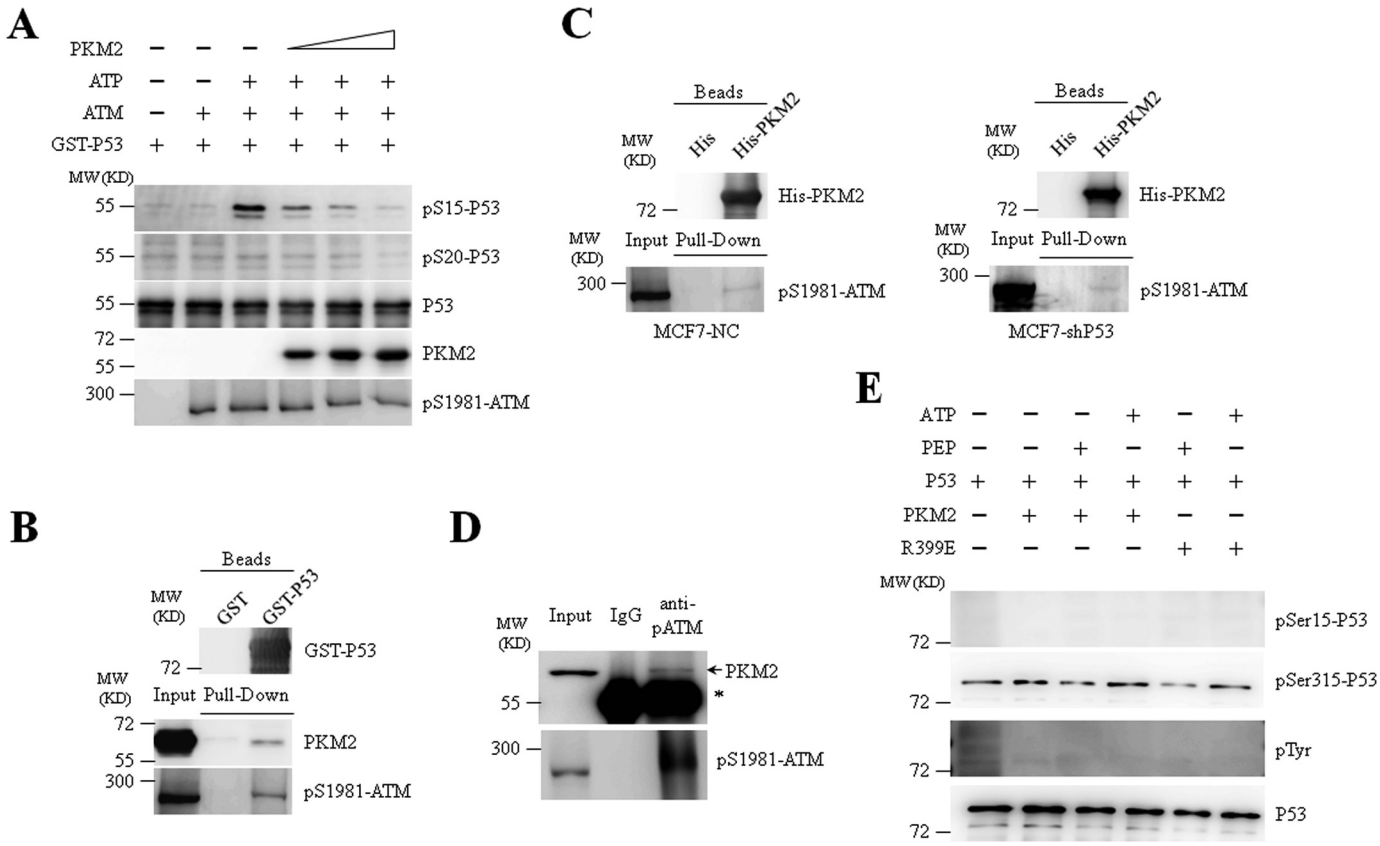

FIGURE 7. **PKM2 inhibits the phosphorylation of P53 by ATM.** *A*, phosphorylation of GST-P53 by ATM in the presence of escalating concentration of recombinant PKM2 was analyzed by the *in vitro* kinase assay. Immunoblots were performed for indicated proteins. pS1981-ATM: anti-Ser-1981-phosphorylated ATM antibody. *B*, GST pull-down assays were performed with GST or GST-P53 and lysate prepared from MCF7 cells treated with etoposide for 8 h. *C*, pull-down assays were performed with His or His-PKM2 and lysates prepared from MCF7 cells, which were infected with NC or shP53 and treated with etoposide for 8 h. *D*, co-IP assays were performed with anti-Ser-1981-phosphorylated ATM antibody in MCF7 cells treated with etoposide for 1 h. IgG was a negative control. Input, 10% the whole cell lysate. * indicates IgG heavy chain band. *E*, purified recombinant PKM2-WT or PKM2-R399E mutant was incubated with recombinant GST-P53 in the presence of PEP or ATP. pSer15-P53, pSer315-P53, pan-phosphothreonine proteins, and P53 were detected by immunoblotting.

Discussion

Cells are constantly confronted with intrinsic and extrinsic genotoxic insults, which can lead to a plethora of different modifications in the physicochemical structure of DNA, placing DDR in a paramount position of importance (34). Dysfunctions in the DDR, either in the control of cell cycle checkpoint such as P53 or in the DNA repair system, will permit the survival or the continued growth of cells with genetic abnormalities, thereby leading to genome instability and malignant transformation (35). In the present study, we show that PKM2 interacts with P53 and negatively modulates its transcriptional activity. Notably, PKM2 depletion alone does not show pronounced effects on cell cycle and growth of wild type P53-bearing MCF7 cells, which is consistent with a previous report demonstrating the absence of oncogenic role of PKM2 in wild type P53-carrying cancer cell lines (RKO, HCT116, and A549) (12). However, PKM2 deletion facilitates DNA damage stimulus-induced cell cycle arrest and decreases proliferation of tumor cells upon DNA damage stimuli. Moreover, xenograft experiments displayed that the knockdown of PKM2 significantly inhibits the *in vivo* growth of MCF7 cells in the presence of DNA damage, which accumulates functional P53. These results suggest that P53 is involved in the decreased tumor growth in PKM2-depleted cells under DNA damage. Indeed, we found that PKM2 physically interacts with P53 and is recruited to the promoter of P53-targeted gene *P21* to inhibit its transcription upon DNA damage. Previous studies demonstrated a co-activating function of PKM2 toward β-catenin and HIF-1α under EGF treatment and hypoxia, respectively (10, 11). However, our data indicate that PKM2 is acting as a corepressor for P53. Although selective transactivation of P53 target genes has been reported previously (36), it deserves to be further investigated how PKM2 mainly inhibited P53-dependent *P21* transcription. Collectively, we propose that expression of PKM2 in tumors inhibits its P53-dependent transactivation by preventing P53 binding to the *P21* promoter, which will allow the cells to continue growing despite the occurrence of DNA damage, endowing the cells with the ability to withstand DNA damage stress and high risk of genome instability.

Mutation of P53 occurs in more than 50% of all cancer types. In this half of human tumors, P53 gene is mutated or functionally inactivated, in which a large part of mutants leading to defect of DNA binding capacity and thereby the transcriptional activity (26, 35). Therefore, further investigations are required to understand how PKM2 modulates DNA damage signaling and tumor growth in the context of a transcriptional inactivated P53. Using GST-pull down assay, we have detected the interaction between purified PKM2 and seven most frequently

happened mutations of P53.[5] Interestingly, the interaction exists in several cases, indicating that PKM2 may also play a role in regulating DNA damage signaling in the context of a transcriptional inactivated P53.

ATM has been shown to play a central role in orchestrating signaling networks including DNA damage, DNA repair and cell cycle control by interacting with and phosphorylating a broad range of substrates. Besides P53, over 1,000 proteins were identified in proteomic screen as putative ATM substrates (37). PKM2 exhibits inhibitory effect on kinase activity of ATM toward P53, although PKM2 does not directly phosphorylate P53. Because interaction between PKM2 and ATM is observed in our experiments, how they interfere with each other in terms of individual substrate deserves to be investigated.

In conclusion, our data suggest a novel functional role for PKM2 in mediating DNA damage signaling by inhibiting the transcriptional activity of checkpoint protein P53 under DNA damage stimuli, through which PKM2 contributes to cancer development. These findings also highlight a role of PKM2 in facilitating cancer cells to survive chemotherapy, the application of DNA damage in treating diseases, making it a new target in preventing cancer development and chemotherapy resistance (38).

Experimental Procedures

Cell Culture—Human MCF7 cells were maintained in Dulbecco's Modified Eagle's Medium (DMEM) supplemented with 10% fetal bovine serum (FBS). MCF7 cells were cultured with 0.01 mg/ml human recombinant insulin (Sigma). For triggering DDR, MCF7 cells were treated with 100 μM etoposide. Human HCT116 and U2OS cells were maintained in Dulbecco's Modified Eagle's Medium (DMEM) supplemented with 10% fetal bovine serum (FBS). For triggering DDR, cells were treated with 100 μM etoposide.

Materials—Etoposide was purchased from Calbiochem. Fructose 1,6-bisphosphate (FBP), phosphoenolpyruvic acid (PEP), adenosine diphosphate (ADP), adenosine triphosphate (ATP), hygromycin B, DNase-free RNase A, and propidium iodide were purchased from Sigma.

Antibodies—Rabbit polyclonal antibodies against PKM2, phospho-p53 (Ser-15), phospho-p53 (Ser-20), ATM, phospho-ATM (Ser-1981), and mouse monoclonal antibodies against P53 and β-actin were obtained from Cell Signaling Technology. Rabbit antibody recognizing P53 and goat antibody against LaminB were obtained from Santa Cruz Biotechnology (Santa Cruz). Rabbit antibody against P21 was from Proteintech Group. Monoclonal antibodies for His and GST were from Sigma.

Cell Transfection—For transient transfection, Lipofectamine 2000 transfection reagent was used following the manufacturer's protocol (Invitrogen). Retroviruses were prepared by transient co-transfection with helper plasmids into 293T cells using Lipofectamine 2000. After the transfection, 1 μg/ml of puromycin was added to screen stable cell lines for further assays.

Vector Construction—Human PKM2 cDNA was amplified from MCF7 cells by RT-PCR and then cloned into psumo3 vector provided by Dr Zhou to construct His-tagged PKM2 protein-expressing plasmid or into pBabe vector (Clontech) to generate psumo3-PKM2 and pbabe-PKM2. Fragments (1–44, 45–116, 117–218, 219–389, and 390–531) of PKM2 cDNA were amplified and constructed by PCR from psumo3-PKM2 plasmids. Human P53 cDNA was amplified from 293T cells by RT-PCR and then cloned into pGEX-6P1 vector. Fragments (1–43, 44–102, 103–300, and 301–393) of P53 cDNA were amplified by PCR from pGEX-P53 plasmids. PKM2 R399E point mutant was created utilizing QuickChange Site-directed Mutagenesis Kit (Stratagene). pSIREN PKM2 shRNA was generated using CATCTACCACTTGCAATTA oligonucleotide targeting transcript of exon 10 of the PKM (4) . Non-sense mutations of C1170T, C1173T, T1174C, and G1176T of PKM2 (4) were cloned into the Rescuing plasmids pQCXIN Retrovial (Clontech). The sequences of all cDNA inserts of plasmids were confirmed by sequencing.

Subcellular Fractionation—Cells were lysed in hypotonic buffer (10 mM Tris-HCl, pH 7.9, 1.5 mM $MgCl_2$, 10 mM KCl, 1 mM DTT, 1 tablet/10 ml EDTA-free complete protease inhibitor mixture (Roche), and 1 tablet/10 ml phosphatase inhibitor mixture (Roche)) by a Dounce homogenizer (40 strokes). Nuclear pellets were separated from cytoplasm by centrifugation for 10 min at 1000 $\times$ *g*. The supernatants (cytoplasmic extract) were removed and transferred into new tubes. Nuclear pellets were washed with hypotonic buffer twice, and resuspended in the nuclear extraction buffer (50 mM Tris-HCl, pH 7.9, 1 mM $MgCl_2$, 1 mM DTT, 0.1% Nonidet P-40, 250 units/ml Benzonase (Sigma), 1 tablet/10 ml EDTA-free complete protease inhibitor mixture and 1 tablet/10 ml phosphatase inhibitor mixture) by sonication. The supernatants (nuclear extracts) were centrifuged for 10 min at 12,000 $\times$ *g*.

Immunoprecipitation Analysis—Whole-cell extracts were prepared in 300 μl of lysis buffer (50 mM HEPES, 50 mM NaCl, 0.1% Tween20, 10% glycerol, 20 mM sodium pyrophosphate, 1 mM dithiothreitol, plus protease inhibitors) and incubated overnight with indicated antibodies (including anti-PKM2 or anti-P53) and protein A/G plus-agarose (Santa Cruz Biotechnology) at 4 °C. After IP, the beads were intensively washed with washing buffer (50 mM Tris-HCl, pH 7.6; 300 mM NaCl; 1 mM EDTA; 0.5% Nonidet P-40; 10% glycerol). Then the precipitates were analyzed by Western blot.

In-solution Digestion (FASP (39))—Eluted proteins from immunoprecipitation were dissolved by denaturation buffer (8 M urea, 0.1 M Tris-HCl, pH 8.5) and centrifuged for 20 min at 14,000 $\times$ *g* at 20 °C in YM-10 filter units for three times. Mixed protein lysates were reduced for 1 h at room temperature by addition of a final concentration of 10 mM dithiothreitol (DTT) and then alkylated for 1 h at room temperature in the dark by addition of a final concentration of 55 mM iodoacetamide (IAA). The urea solvent of the protein mixtures were exchanged with 50 mM NH_4HCO_3 by centrifugation for 20 min at 14,000 $\times$ *g* at 20 °C for three times, followed by protein digestion with sequencing grade modified trypsin (Promega) at a protein-to-enzyme of 50:1 at 37 °C overnight. Tryptic peptides were collected by centrifuge for 20 min at 14,000 $\times$ *g* at 20 °C.

LC-MS/MS Analysis—The eluted peptides were lyophilized using a SpeedVac (ThermoSavant), and resuspended in 10 μl of

[5] Y. Lu, unpublished data.

1% formic acid/5% acetonitrile. All mass spectrometric experiments are performed on a LTQ orbitrap "XL" mass spectrometer connected to an Easy-nLC 1000 via an Easy Spray (Thermo Fisher Scientific). The peptide mixture was loaded onto a 50 cm with 0.075-mm inner diameter column packed with C18 2-μm Reversed Phase resins (PepMap RSLC), and separated within a 300 min linear gradient from 95% solvent A (0.1% formic acid/2% acetonitrile/98% water) to 35% solvent B (0.1% formic acid/100% acetonitrile) at a flow rate of 200 nl/min. The spray voltage was set to 2 kV and the temperature of ion transfer capillary was 180 °C. The mass spectrometer was operated in positive ion mode and employed in the data-dependent mode to automatically switch between MS and MS/MS using the Tune and Xcalibur 2.5.5 software package. One full MS scan from 350 to 1800 m/z was acquired at high resolution r = 100,000 (defined at m/z = 400), followed by fragmentation of the ten most abundant multiply charged ions (singly charged ions and ions with unassigned charge states were excluded).

Gene Ontology(GO) Analysis—The annotation tools DAVID 6.7 (40) (david.abcc.ncifcrf.gov/home.jsp) was used for functional annotation and GO enrichment analysis of phosphoproteins. The p value threshold was kept below 0.01.

Purification of Recombinant Proteins—His-tagged (pSUMO3 vector) WT and mutant PKM2 were expressed in bacteria BL21 (DE3) by induction with 0.5 mM isopropylthiogalactopyranoside (IPTG) at 30 °C and purified from the cytosol of the expressed cells by affinity chromatography on Ni-NTA-agarose (Qiagen). The GST-P53 or its mutants were expressed in BL21 by induction with IPTG at 28 °C and purified using Bulk and RediPack GST Purification Modules (Amersham Biosciences).

Size-Exclusion Chromatography—The bacterially purified PKM2 or P53 protein was loaded into a Superdex 200 10/300GL column and eluted with elution buffer (50 mM phosphate, 0.15 M NaCl, pH 7.2). Each 300-μl consecutive fraction was collected, and 20 μl of each fraction was analyzed by immunoblots.

GST Pull-down Assays—The purified PKM2 proteins were incubated with GST-tagged P53 protein for 30 min at room temperature. Then the precipitations were washed with buffer containing 700 μM NaCl, eluted by the SDS sample buffer, and analyzed by immunoblots.

Western Blots—Protein extracts were equally loaded on 10–12% SDS-polyacrylamide gel, and transferred to nitrocellulose membrane (Amersham Bioscience). The blots were stained with 0.2% Ponceau S red to ensure equal protein loading. After blocking with 5% nonfat milk in PBS, the membranes were incubated with indicated antibodies, followed by horseradish perioxidase (HRP)-linked secondary antibodies (Cell Signaling). Detection was performed by chemiluminescence phototope-HRP kit (Cell Signaling).

Confocal Microscopy—Cells were treated as described in the text, harvested on slides and fixed. After permeabilization with 0.1% (v/v) Triton X-100 in PBS and blocking with 2% (w/v) BSA in PBS, cells were incubated overnight with the indicated antibodies followed by secondary antibodies conjugated either with Alexa Fluor 555 dye (Invitrogen) or Alexa Fluor 488 dye for 1 h. Cellular DNA was counterstained with 4,6-diamidino-2-phenylindole (DAPI; Molecular Probes). Fluorescence signals were detected on a Nikon A1R confocal laser microscope.

Luciferase Reporter Assays—MCF7 cells (WT or PKM2-depleted) were seeded onto 24-well plates, transfected with pp53-TA-firefly-luc reporter (Beyotime Institute of Biotechnology) and control reporter pSV40-*Renilla* together. The pp53-TA-firefly-luc reporter was constructed by inserting multiple P53 response elements in PGL6-TA vector. Firefly Luc and *Renilla* Luc activities were determined using the Dual-Luciferase Assay System (Promega).

ChIP Assays—ChIP assays were performed with a Pierce Agarose ChIP Kit (26156, Pierce Biotechnology) in accordance with the manufacturer's instructions. Normal rabbit IgG was used as negative control. DNA was immunoprecipitated and analyzed by SYBR Green Real-time PCR (ABI PRISM 7900) with the primers in the promoter of the P21 gene (41).

Real-time Quantitative RT-PCR—Total cellular RNA from cell lines was extracted by TRIzol reagent (Invitrogen) and treated with RNase-free DNase (Promega). Complementary DNA (cDNA) was synthesized using the cDNA synthesis kit according to the manufacturer's instruction (Applied Biosystems, Foster City, CA). Real-time RT-PCR was performed and data were analyzed according to our previous report (42). Specific oligonucleotide primers for P21 (43), GADD45 (44), MDM2 (43), and 14-3-3σ (29) were used and listed below. β-Actin cDNA was amplified as internal positive controls (sense, 5′-CATCCTCACCCTGAAGTACCC-3′, antisense, 5′-AGCCTGGATAGCAACGTACATG-3′).

P21-F: 5′-TGCGTTCACAGGTGTTTCTG-3′, P21-R: 5′-GTCCACTGGGCCGAAGAG-3′; GADD45-F: 5′-TCAGCGCACGATCACTGTC-3′, GADD45-R: 5′-CCAGCAGGCACAACACCAC-3′; MDM2-F: 5′-GGCAGGGGAGAGTGATACAGA-3′, MDM2-R: 5′-GAAGCCAATTCTCACGAAGGG-3′; 14-3-3σ-F: 5′-CCTGCTGGACAGCCACCTCA-3′, 14-3-3σ-R: 5′-TGTCGGCCGTCCACAGTGTC-3′.

Cell Cycle Analysis—Cells were collected, rinsed, and fixed overnight in 75% cold ethanol at −20 °C. Following treatment with 1% RNase, cells were stained with 50 mg/ml propidium iodide (PI, Sigma-Aldrich). Cell-cycle distribution was determined by flow cytometry (Beckman Coulter, Miami, FL).

Measurements of Glucose Uptake—MCF7 cells (WT or PKM2-depleted) were seeded in culture dishes and were grown under normal conditions for 24 h. Then 100 μM 2-NBDG (Invitrogen) was added to the culture medium and plates were incubated at 37 °C with 5% CO_2 for 15 min. Fluorescence was measured in a FACS Calibur Analyzer (BD). Glucose uptake was normalized by cell numbers (per 10^6).

Animal Experiments—All animal experiments were performed with the approval of the committee for humane treatment of animals at Shanghai Jiao Tong University School of Medicine. The 6–8-week-old female nude mice (Slaccas Laboratory Animal, Shanghai, China) were supplemented with 0.36 mg of 60-day release 17β-estradiol pellets (Innovative Research, Novi, MI) by subcutaneous inoculation. Then, 5×10^6 MCF7 cells infected with NC or shPKM2#1 were injected into the mammary fat pad of the mice under isofluorane. Three weeks after injection, bioluminescence imaging was used to monitor the tumor growth. Next, etoposide was administrated intraperitoneally for 7 consecutive days. Two

weeks later, bioluminescent imaging was performed using the Xenogen IVIS Imaging System.

Measurement of Pyruvate, Lactate, PEP, and Pyruvate Kinase Activity—Levels of pyruvate, lactate, and PEP were determined using Pyruvate Colorimetric/Fluorometric Assay Kit, Lactate Colorimetric/Fluorometric Assay Kit, and PEP Colorimetric/Fluorometric Assay Kit (Biovision), respectively. The pyruvate kinase activity was measured using Pyruvate Kinase Activity Colorimetric/Fluorometric Assay Kit (Biovision).

In Vitro Kinase Assay—Bacterially purified His-tagged recombinant PKM2 or ATM were incubated with GST-tagged P53 (10 μg/ml) in 50 μl of kinase buffer (Cell Signaling Technology) with PEP or ATP at 25 °C for 2 h. The reactions were terminated by addition of SDS loading buffer and heated to 100 °C. The reaction mixtures were then analyzed by SDS-PAGE.

Statistical Analysis—The Student's *t* test was used to compare the difference between two different groups. A value of $p < 0.05$ was considered to be statistically significant.

Author Contributions—L. X., Y. L., and G.-Q. C. designed research; L. X., X.-R. W., X.-L. W., S.-H. L., X.-W. D., and Y. L. performed research; L. X., X.-R. W., and Y. L. contributed new reagents/analytic tools; L. X., and Y. L. analyzed data; and Y. L., and G.-Q. C. wrote the paper.

Acknowledgment—We thank Dr. Ai-Wu Zhou for the psumo3 vector.

References

1. Ashizawa, K., Willingham, M. C., Liang, C. M., and Cheng, S. Y. (1991) *In vivo* regulation of monomer-tetramer conversion of pyruvate kinase subtype M2 by glucose is mediated via fructose 1,6-bisphosphate. *J. Biol. Chem.* **266,** 16842–16846
2. Ikeda, Y., Tanaka, T., and Noguchi, T. (1997) Conversion of non-allosteric pyruvate kinase isozyme into an allosteric enzyme by a single amino acid substitution. *J. Biol. Chem.* **272,** 20495–20501
3. Christofk, H. R., Vander Heiden, M. G., Harris, M. H., Ramanathan, A., Gerszten, R. E., Wei, R., Fleming, M. D., Schreiber, S. L., and Cantley, L. C. (2008) The M2 splice isoform of pyruvate kinase is important for cancer metabolism and tumour growth. *Nature* **452,** 230–233
4. Yang, W., Xia, Y., Hawke, D., Li, X., Liang, J., Xing, D., Aldape, K., Hunter, T., Alfred Yung, W. K., and Lu, Z. (2012) PKM2 phosphorylates histone H3 and promotes gene transcription and tumorigenesis. *Cell* **150,** 685–696
5. Keller, K. E., Doctor, Z. M., Dwyer, Z. W., and Lee, Y. S. (2014) SAICAR induces protein kinase activity of PKM2 that is necessary for sustained proliferative signaling of cancer cells. *Mol Cell* **53,** 700–709
6. Gao, X., Wang, H., Yang, J. J., Liu, X., and Liu, Z. R. (2012) Pyruvate kinase M2 regulates gene transcription by acting as a protein kinase. *Mol. Cell* **45,** 598–609
7. Gao, X., Wang, H., Yang, J. J., Chen, J., Jie, J., Li, L., Zhang, Y., and Liu, Z. R. (2013) Reciprocal regulation of protein kinase and pyruvate kinase activities of pyruvate kinase M2 by growth signals. *J. Biol. Chem.* **288,** 15971–15979
8. Jiang, Y., Li, X., Yang, W., Hawke, D. H., Zheng, Y., Xia, Y., Aldape, K., Wei, C., Guo, F., Chen, Y., and Lu, Z. (2014) PKM2 regulates chromosome segregation and mitosis progression of tumor cells. *Mol. Cell* **53,** 75–87
9. Jiang, Y., Wang, Y., Wang, T., Hawke, D. H., Zheng, Y., Li, X., Zhou, Q., Majumder, S., Bi, E., Liu, D. X., Huang, S., and Lu, Z. (2014) PKM2 phosphorylates MLC2 and regulates cytokinesis of tumour cells. *Nat. Commun.* **5,** 5566
10. Yang, W., Zheng, Y., Xia, Y., Ji, H., Chen, X., Guo, F., Lyssiotis, C. A., Aldape, K., Cantley, L. C., and Lu, Z. (2012) ERK1/2-dependent phosphorylation and nuclear translocation of PKM2 promotes the Warburg effect. *Nat. Cell Biol.* **14,** 1295–1304
11. Luo, W., Hu, H., Chang, R., Zhong, J., Knabel, M., O'Meally, R., Cole, R. N., Pandey, A., and Semenza, G. L. (2011) Pyruvate kinase M2 is a PHD3-stimulated coactivator for hypoxia-inducible factor 1. *Cell* **145,** 732–744
12. Cortés-Cros, M., Hemmerlin, C., Ferretti, S., Zhang, J., Gounarides, J. S., Yin, H., Muller, A., Haberkorn, A., Chene, P., Sellers, W. R., and Hofmann, F. (2013) M2 isoform of pyruvate kinase is dispensable for tumor maintenance and growth. *Proc. Natl. Acad. Sci. U.S.A.* **110,** 489–494
13. Israelsen, W. J., Dayton, T. L., Davidson, S. M., Fiske, B. P., Hosios, A. M., Bellinger, G., Li, J., Yu, Y., Sasaki, M., Horner, J. W., Burga, L. N., Xie, J., Jurczak, M. J., DePinho, R. A., Clish, C. B., Jacks, T., Kibbey, R. G., Wulf, G. M., Di Vizio, D., Mills, G. B., Cantley, L. C., and Vander Heiden, M. G. (2013) PKM2 isoform-specific deletion reveals a differential requirement for pyruvate kinase in tumor cells. *Cell* **155,** 397–409
14. Wang, Y. H., Israelsen, W. J., Lee, D., Yu, V. W., Jeanson, N. T., Clish, C. B., Cantley, L. C., Vander Heiden, M. G., and Scadden, D. T. (2014) Cell-state-specific metabolic dependency in hematopoiesis and leukemogenesis. *Cell* **158,** 1309–1323
15. Goldberg, M. S., and Sharp, P. A. (2012) Pyruvate kinase M2-specific siRNA induces apoptosis and tumor regression. *J. Exp. Med.* **209,** 217–224
16. Bluemlein, K., Grüning, N. M., Feichtinger, R. G., Lehrach, H., Kofler, B., and Ralser, M. (2011) No evidence for a shift in pyruvate kinase PKM1 to PKM2 expression during tumorigenesis. *Oncotarget* **2,** 393–400
17. Wade, M., Li, Y. C., and Wahl, G. M. (2013) MDM2, MDMX and p53 in oncogenesis and cancer therapy. *Nature Reviews. Cancer* **13,** 83–96
18. Haupt, Y., Maya, R., Kazaz, A., and Oren, M. (1997) Mdm2 promotes the rapid degradation of p53. *Nature* **387,** 296–299
19. Kruse, J. P., and Gu, W. (2009) Modes of p53 regulation. *Cell* **137,** 609–622
20. Meek, D. W. (2009) Tumour suppression by p53: a role for the DNA damage response? *Nature Reviews. Cancer* **9,** 714–723
21. Anastasiou, D., Yu, Y., Israelsen, W. J., Jiang, J. K., Boxer, M. B., Hong, B. S., Tempel, W., Dimov, S., Shen, M., Jha, A., Yang, H., Mattaini, K. R., Metallo, C. M., Fiske, B. P., Courtney, K. D., Malstrom, S., Khan, T. M., Kung, C., Skoumbourdis, A. P., Veith, H., Southall, N., Walsh, M. J., Brimacombe, K. R., Leister, W., Lunt, S. Y., Johnson, Z. R., Yen, K. E., Kunii, K., Davidson, S. M., Christofk, H. R., Austin, C. P., Inglese, J., Harris, M. H., Asara, J. M., Stephanopoulos, G., Salituro, F. G., Jin, S., Dang, L., Auld, D. S., Park, H. W., Cantley, L. C., Thomas, C. J., and Vander Heiden, M. G. (2012) Pyruvate kinase M2 activators promote tetramer formation and suppress tumorigenesis. *Nat. Chem. Biol.* **8,** 839–847
22. Christofk, H. R., Vander Heiden, M. G., Wu, N., Asara, J. M., and Cantley, L. C. (2008) Pyruvate kinase M2 is a phosphotyrosine-binding protein. *Nature* **452,** 181–186
23. Hathurusinghe, H. R., Goonetilleke, K. S., and Siriwardena, A. K. (2007) Current status of tumor M2 pyruvate kinase (tumor M2-PK) as a biomarker of gastrointestinal malignancy. *Ann. Surg. Oncol* **14,** 2714–2720
24. Iliakis, G., Wang, Y., Guan, J., and Wang, H. (2003) DNA damage checkpoint control in cells exposed to ionizing radiation. *Oncogene* **22,** 5834–5847
25. Nagasawa, H., Li, C. Y., Maki, C. G., Imrich, A. C., and Little, J. B. (1995) Relationship between radiation-induced G1 phase arrest and p53 function in human tumor cells. *Cancer Res.* **55,** 1842–1846
26. Muller, P. A., and Vousden, K. H. (2013) p53 mutations in cancer. *Nat. Cell Biol.* **15,** 2–8
27. Zhang, H., Somasundaram, K., Peng, Y., Tian, H., Zhang, H., Bi, D., Weber, B. L., and El-Deiry, W. S. (1998) BRCA1 physically associates with p53 and stimulates its transcriptional activity. *Oncogene* **16,** 1713–1721
28. Kamijo, T., Weber, J. D., Zambetti, G., Zindy, F., Roussel, M. F., and Sherr, C. J. (1998) Functional and physical interactions of the ARF tumor suppressor with p53 and Mdm2. *Proc. Natl. Acad. Sci. U.S.A.* **95,** 8292–8297
29. Akahira, J., Sugihashi, Y., Suzuki, T., Ito, K., Niikura, H., Moriya, T., Nitta, M., Okamura, H., Inoue, S., Sasano, H., Okamura, K., and Yaegashi, N. (2004) Decreased expression of 14–3-3 sigma is associated with advanced disease in human epithelial ovarian cancer: its correlation with aberrant DNA methylation. *Clin. Cancer Res.* **10,** 2687–2693

30. Jenkins, L. M., Durell, S. R., Mazur, S. J., and Appella, E. (2012) p53 N-terminal phosphorylation: a defining layer of complex regulation. *Carcinogenesis* **33,** 1441–1449
31. Pabla, N., Huang, S., Mi, Q. S., Daniel, R., and Dong, Z. (2008) ATR-Chk2 signaling in p53 activation and DNA damage response during cisplatin-induced apoptosis. *J. Biol. Chem.* **283,** 6572–6583
32. Fernandez-Capetillo, O., Chen, H. T., Celeste, A., Ward, I., Romanienko, P. J., Morales, J. C., Naka, K., Xia, Z., Camerini-Otero, R. D., Motoyama, N., Carpenter, P. B., Bonner, W. M., Chen, J., and Nussenzweig, A. (2002) DNA damage-induced G2-M checkpoint activation by histone H2AX and 53BP1. *Nat. Cell Biol.* **4,** 993–997
33. Yang, W., Xia, Y., Ji, H., Zheng, Y., Liang, J., Huang, W., Gao, X., Aldape, K., and Lu, Z. (2011) Nuclear PKM2 regulates beta-catenin transactivation upon EGFR activation. *Nature* **480,** 118–122
34. Cao, L. L., Shen, C., and Zhu, W. G. (2016) Histone modifications in DNA damage response. *Science China. Life Sciences* **59,** 257–270
35. Kastan, M. B., and Bartek, J. (2004) Cell-cycle checkpoints and cancer. *Nature* **432,** 316–323
36. Bouvard, V., Zaitchouk, T., Vacher, M., Duthu, A., Canivet, M., Choisy-Rossi, C., Nieruchalski, M., and May, E. (2000) Tissue and cell-specific expression of the p53-target genes: bax, fas, mdm2 and waf1/p21, before and following ionising irradiation in mice. *Oncogene* **19,** 649–660
37. Matsuoka, S., Ballif, B. A., Smogorzewska, A., McDonald, E. R., 3rd, Hurov, K. E., Luo, J., Bakalarski, C. E., Zhao, Z., Solimini, N., Lerenthal, Y., Shiloh, Y., Gygi, S. P., and Elledge, S. J. (2007) ATM and ATR substrate analysis reveals extensive protein networks responsive to DNA damage. *Science* **316,** 1160–1166
38. Papadaki, C., Sfakianaki, M., Lagoudaki, E., Giagkas, G., Ioannidis, G., Trypaki, M., Tsakalaki, E., Voutsina, A., Koutsopoulos, A., Mavroudis, D., Georgoulias, V., and Souglakos, J. (2014) PKM2 as a biomarker for chemosensitivity to front-line platinum-based chemotherapy in patients with metastatic non-small-cell lung cancer. *Br. J. Cancer* **111,** 1757–1764
39. Winiewski, J. R., Zougman, A., Nagaraj, N., and Mann, M. (2009) Universal sample preparation method for proteome analysis. *Nature Methods* **6,** 359–362
40. Huang, Da W., Sherman, B. T., and Lempicki, R. A. (2009) Systematic and integrative analysis of large gene lists using DAVID bioinformatics resources. *Nature Protocols* **4,** 44–57
41. Huang, H., Liu, N., Yang, C., Liao, S., Guo, H., Zhao, K., Li, X., Liu, S., Guan, L., Liu, C., Xu, L., Zhang, C., Song, W., Li, B., Tang, P., Dou, Q. P., and Liu, J. (2012) HDAC inhibitor L-carnitine and proteasome inhibitor bortezomib synergistically exert anti-tumor activity *in vitro* and *in vivo*. *PLoS ONE* **7,** e52576
42. Lu, Y., Xu, Y. B., Yuan, T. T., Song, M. G., Lübbert, M., Fliegauf, M., and Chen, G. Q. (2006) Inducible expression of AML1-ETO fusion protein endows leukemic cells with susceptibility to extrinsic and intrinsic apoptosis. *Leukemia* **20,** 987–993
43. Cui, D., Li, L., Lou, H., Sun, H., Ngai, S. M., Shao, G., and Tang, J. (2014) The ribosomal protein S26 regulates p53 activity in response to DNA damage. *Oncogene* **33,** 2225–2235
44. Shandilya, J., Wang, Y., and Roberts, S. G. (2012) TFIIB dephosphorylation links transcription inhibition with the p53-dependent DNA damage response. *Proc. Natl. Acad. Sci. U.S.A.* **109,** 18797–18802